An alternative method for calculation of *Rayleigh* and *Love* wave phase velocities by using three-component records on a single circular array without a central station

Antonio García-Jerez, Francisco Luzón, Manuel Navarro

Department of Applied Physics, University of Almería, Cañada de San Urbano s/n, 04120 Almería, Spain. E-mail: agj574@ual.es

Accepted *2008 Feb 14*. Received *2008 Feb 14*; in original form *2007 Apr 9*

Short Title: Single circular array method

Contact Address:

Antonio García Jerez

Department of Applied Physics. University of Almería.

Cañada de San Urbano s/n

CP 04120 Almería, Spain.

E-mail: agj574@ual.es Fax : +34 950 01 54 77

SUMMARY

A method for the computation of phase velocities of surface waves from microtremor waveforms is shown. The technique starts from simultaneous three-component records obtained in a circular array without a central station. Then, Fourier spectra of vertical, radial and tangential components of motion are calculated for each station and considered as complex-valuated functions of the azimuthal coordinate. A couple of intermediate real physical quantities, B and C, can be defined from the 0 and ± 1– order coefficients of the Fourier series expansion of such functions. Finally, phase velocities of *Rayleigh* and *Love* waves can be retrieved from B and C by solving respective one-unknown equations. The basic assumption is the possibility of expanding the wavefield as a sum of plane surface waves with *Rayleigh* and *Love* wavenumbers being univocal functions of the circular frequency. The method is tested in synthetic ambient noise wavefields confirming its reliability and robustness for passive seismic surveying.

Key words: seismic noise, seismic array, seismology, surface waves

1 INTRODUCTION

Seismic surveying methods based on surface waves have been widely shown as powerful tools for the determination of ground structures, by themselves or together with other geophysical techniques (see for example Noguchi & Nishida 2002; Sakai & Morikawa 2006). Since the earlier work of Aki (1957), methods based on study of propagation of ambient noise (microtremor), consisting of elastic waves generated by environmental sources, have been popularized. That paper has been considered the basis of a group of techniques named as SPatial AutoCorrelation methods (SPAC) for the calculation of dispersion curves of surface waves which represent an intermediate stage for estimation of ground structures in terms of its elastodynamic parameters.

The more widely used theoretical scheme of the SPAC method requires the acquisition of vertical motion records on a set of stations located along a circumference and at its centre for the calculation of *Rayleigh* wave dispersion curves. Although the fundamental equations were derived for infinitely dense circular arrays, the SPAC method can also be applied for real arrays with finite number of sensors for a wavelength range depending on the array size and wavefield characteristics (see Okada 2006). The precision and sufficiency of measurements of structure-dependent physical quantities represent a decisive influence on the accuracy of the inverted physical models of the earth

crust. Thus, seismologists are encouraged to obtain the higher performance from microtremor records, using them for the estimation of as many relevant characteristics of surface waves as possible. In this context, *Rayleigh* wave velocity and ellipticity, as well as *Love* wave dispersion curve are physical quantities of special interest and should be used together for the inversion of better constrained ground models considering their predominant sensitivities to different structural characteristics. Advanced inversion schemes taking advantage of this can be found in the literature (Métaxian & Lesage 1997; Parolai *et al.* 2005; Arai & Tokimatsu 2005; Wathelet 2005; Köhler *et al.* 2007; García-Jerez *et al*. 2008; among others). Many efforts are also devoted to the development and improvement of techniques for experimental calculation of surface wave characteristics. The three-component SPAC method (3c-SPAC, see Appendix A) is a variant of SPAC permitting calculation of both types of surface wave velocities from three-component microtremor records obtained in a circular array with a central station. This was also pointed out by Aki (1957). Further studies by Okada & Matsushima (1989) and Morikawa (2006) provided a detailed derivation in the general case of wavefields composed of both types of surface waves with arbitrary relative power. An extension of that technique by relaxing the hypothesis of perfect circular array has been developed and tested by Köhler *et al.* (2007). In recent works, Cho *et al.* (2006a) and García-Jerez *et al.*

(2006a and 2008) proposed similar methods for the calculation of both *Rayleigh* and *Love* wave dispersion curves by horizontal-component microtremor recorded in a double circular array.

The aim of this work is to present an alternative approach for the computation of *Rayleigh* and *Love* phase velocities from three-component microtremor records on a single circular array without a central station. This technique, named hereafter as SCAM (Single Circular Array Method), is based on the calculation of a couple of intermediate quantities which can be related to both surface wave velocities. The mathematical derivation is presented for a wavefield written as an arbitrary sum of plane surface waves. Finally, numerical simulations for both the SCAM and the 3c-SPAC method have been compared.

2 METHOD

2.1 REPRESENTATION OF THE WAVEFIELD

Two basic suppositions about the composition of the incident wavefield will be assumed in the following calculations:

i) The wavefield can be represented as a discrete sum of plane surface wavefronts.

ii) Surface waves show a clearly predominant mode for each frequency and type of

wave (*Rayleigh* or *Love*).

The plane wave hypothesis holds only when distances from the sources to the array centre are large enough in comparison with its radius, so that, the curvature of the wavefront and the subsequent drop of energy through the array due to the geometrical attenuation might be neglected. Hypothesis ii) implies that unambiguous frequency vs. phase velocity relations can be defined for both *Rayleigh* and *Love* surface waves since frequency bands for which several modes coexist are not considered. Thus, the Fourier-transformed wavefield at any position $\mathbf{r}$ on the ground surface can be expressed as:

$$\mathbf{U}(\mathbf{r},\omega) = \sum_{j=1}^{N} \left[\mathbf{A}_{Rj}(\omega)\, exp(-ik_R(\omega)\, \mathbf{e}_{\varphi_j} \cdot \mathbf{r}) + \mathbf{A}_{Lj}(\omega)\, exp(-ik_L(\omega)\, \mathbf{e}_{\varphi_j} \cdot \mathbf{r}) \right], \qquad (1)$$

where $k_R(\omega)$ and $k_L(\omega)$ represent the wavenumbers of the predominant modes of *Rayleigh* and *Love* waves respectively for the circular frequency ω. The unit radial vector $\mathbf{e}_\varphi = \mathbf{e}_x \cos\varphi + \mathbf{e}_y \sin\varphi$ points to the direction defined by the azimuthal angle φ on the horizontal plane XY (flat ground surface, Fig. 1), and i is the imaginary unit. The complex physical quantities $\mathbf{A}_{Rj}(\omega)$ and $\mathbf{A}_{Lj}(\omega)$ represent the amplitudes of the *Rayleigh* and *Love* plane waves spreading in direction φ_j due to the j-th source. N

Fig. 1

is the total number of distant sources generating the wavefield. The characteristics of the polarization of surface waves yield the following constraints:

$$\mathbf{A}_{Rj}(\omega) = A_{Rj}^{H}(\omega)\mathbf{e}_{\varphi_j} + A_{Rj}^{V}(\omega)\mathbf{e}_z, \tag{2}$$

$$\mathbf{A}_{Lj}(\omega) = A_{Lj}(\omega)\mathbf{e}_z \times \mathbf{e}_{\varphi_j}, \tag{3}$$

$$A_{Rj}^{H}(\omega) / A_{Rj}^{V}(\omega) = -i\chi(\omega) \quad \text{with} \quad \chi(\omega) \quad \text{a real number.} \tag{4}$$

Equation (2) takes into account that motion is constrained to a vertical plane containing the direction of wave propagation for *Rayleigh* waves, while Eq. (3) restricts motion to be horizontal and perpendicular to the propagation direction in the case of *Love* waves. Eq. (4) implies that difference in phases between the vertical and the horizontal components of *Rayleigh* waves is $\pm\pi/2$. Symbol $\chi(\omega)$ represents the ellipticity of the predominant mode of *Rayleigh* waves for the frequency ω. The unit vector $\mathbf{e}_z$ is vertical and directed up, and subscripts H and V refer to horizontal and vertical projections respectively.

2.2 FOURIER SERIES EXPANSION OF THE VERTICAL, RADIAL AND TANGENTIAL COMPONENTS VS. THE AZIMUTHAL COORDINATE

If three-component records of the wavefield were available at any point $R\mathbf{e}_\theta$ on a circumference with radius R, three azimuth-dependent functions may be defined from the Fourier-transformed records in a given time window. These are the vertical component of the wavefield $W(R,\theta,\omega) = \mathbf{e}_z \cdot \mathbf{U}(R\mathbf{e}_\theta,\omega)$, the radial component $U^{rad}(R,\theta,\omega) = \mathbf{e}_\theta \cdot \mathbf{U}(R\mathbf{e}_\theta,\omega)$ and the tangential component $U^{tg}(R,\theta,\omega) = (\mathbf{e}_z \times \mathbf{e}_\theta) \cdot \mathbf{U}(R\mathbf{e}_\theta,\omega)$. These functions are continuous and smooth for the incident wavefield given by Eq. (1). The Fourier-Series coefficients of the expansion of these functions on the azimuthal coordinate θ may be empirically evaluated and theoretically connected to meaningful properties of the wavefield such as the phase velocity of *Love* and *Rayleigh* waves. An early application of the Fourier-Bessel analysis to stationary random processes can be found in the article by Henstridge (1979). The theoretical values for such coefficients can be obtained from Eqs. (1) and (2) to (4) as:

$$W_m(R,\omega) = \int_{-\pi}^{\pi} exp(-im\theta) W(R,\theta,\omega) d\theta = 2\pi(-i)^m A_R^{V,m} J_m(x_R), \qquad (5)$$

$$U_m^{rad}(R,\omega) = (-i)^{m-1}\pi A_R^{H,m}\left(J_{m-1}(x_R) - J_{m+1}(x_R)\right) + (-i)^m \pi A_L^m\left(J_{m-1}(x_L) + J_{m+1}(x_L)\right), \quad (6)$$

$$U_m^{tg}(R,\omega) = -(-i)^m \pi A_R^{H,m}\left(J_{m-1}(x_R) + J_{m+1}(x_R)\right) + (-i)^{m-1}\pi A_L^m\left(J_{m-1}(x_L) - J_{m+1}(x_L)\right), \quad (7)$$

where $x_R(\omega) = k_R(\omega)R$, $x_L(\omega) = k_L(\omega)R$, and the complex coefficients $A_R^{V,m}$, $A_R^{H,m}$ and A_L^m have been defined as:

$$A_R^{V,m}(\omega) = \sum_{j=1}^{N} exp(-im\varphi_j) A_{Rj}^V(\omega), \quad (8)$$

$$A_R^{H,m}(\omega) = \sum_{j=1}^{N} exp(-im\varphi_j) A_{Rj}^H(\omega), \quad (9)$$

$$A_L^m(\omega) = \sum_{j=1}^{N} exp(-im\varphi_j) A_{Lj}(\omega). \quad (10)$$

The integral representation $\int_{-\pi}^{+\pi} exp(-in\theta - ix\cos(\theta-\varphi))d\theta = 2\pi(-i)^n exp(-in\varphi)J_n(x)$ for the n - order Bessel function $J_n(x)$ has been used in the former derivation (Abramowitz & Stegun 1972).

2.3 COMPUTATION OF *RAYLEIGH* AND *LOVE* PHASE VELOCITIES

Several suitable options can be found in order to retrieve phase velocities of *Rayleigh* and *Love* waves and *Rayleigh* wave ellipticity from Eqs. (5) to (7). The possibility of derivation of the signed ellipticity of *Rayleigh* waves has been pointed out in the preliminary work by García-Jerez *et al.* (2006b) based on Eqs. (5) and (6) for $m = 0$ together with Eq. (4). Cho *et al.* (2006a) found a similar method under the hypothesis of random stationary wavefield. García-Jerez *et al.* (2006a) adapted the original theory for stationary random wavefields by Cho *et al.* (2006a) for the deterministic wavefield formulation and obtained *Love* velocities from simultaneous measurements along an array made up of two concentric rings. That method makes use of Eqs. (6) and (7) in the case of $m = 0$, that is, the calculation of the azimuthal average of radial or tangential spectra. The generalization of the SPAC method (Aki 1957) for derivation of *Rayleigh* and *Love* velocities from three-component records (i. e. Morikawa 2006) taking advantage of Eq. (5) for $m = 0$, and Eqs. (6) and (7) for $m = \pm 1$ has been summarized in Appendix A after adaptation to our deterministic and discrete representation of the wavefield. Nevertheless, a different scheme is immediately suggested by the equations (5) to (7), consisting of a joint resolution of them for a unique radius R. Therefore, the requirement of the central station is eliminated. A system of eleven equations involving

the unknowns x_L, x_R, χ, $A_R^{V,-1}$, $A_R^{V,0}$, $A_R^{V,+1}$, $A_R^{H,-1}$, $A_R^{H,0}$, $A_R^{H,+1}$, A_L^{-1} and A_L^{+1} is generated considering Eqs. (5) and (6) for m = -1, 0, 1; and Eq. (7) for $m = -1, +1$ together with Eq. (4) which provides three additional constraints for the ratios $A_R^{H,m} / A_R^{V,m}$ for $m = -1, 0, 1$. Such a set of equations involves eight empirically computable coefficients: W_{-1}, W_0, W_{+1}, U_{-1}^{rad}, U_0^{rad}, U_{+1}^{rad}, U_{-1}^{tg} and U_{+1}^{tg}, from which, the structure-dependent physical quantities x_L, x_R and χ can be worked out.

In a first stage, the system can be simplified by elimination of all variables representing weighted amplitudes of plane waves. It yields (Appendix B):

$$\frac{U_0^{rad}(R,\omega)}{f_0(x_R)W_0(R,\omega)} = \frac{\chi(\omega)}{x_R}, \tag{11}$$

$$\frac{U_{+1}^{rad}(R,\omega)f_1(x_L)+iU_{+1}^{tg}(R,\omega)}{\left[f_1(x_R)f_1(x_L)-1\right]W_{+1}(R,\omega)} = \frac{\chi(\omega)}{x_R}, \tag{12}$$

$$\frac{U_{-1}^{rad}(R,\omega)f_1(x_L)-iU_{-1}^{tg}(R,\omega)}{\left[f_1(x_R)f_1(x_L)-1\right]W_{-1}(R,\omega)} = \frac{\chi(\omega)}{x_R}, \tag{13}$$

where functions $f_m(x)$ have been defined, for any m, as:

$$f_m(x) = \frac{x}{2}\left(J_{m-1}(x)-J_{m+1}(x)\right)/J_m(x) = x\frac{J_{m-1}(x)}{J_m(x)} - m. \tag{14}$$

Fig. 2 The behaviors of functions $f_0(x)$ and $f_1(x)$ have been shown in Fig. 2a for cases $m = 0$ and $m = 1$. Elimination of x_R and χ from Eqs. (12) and (13) yields the x_L-dependent equation:

$$f_1(x_L) = B(R,\omega), \tag{15}$$

with B representing the quantity:

$$B(R,\omega) = i\frac{U_{-1}^{tg}(R,\omega)W_{+1}(R,\omega) + U_{+1}^{tg}(R,\omega)W_{-1}(R,\omega)}{U_{-1}^{rad}(R,\omega)W_{+1}(R,\omega) - U_{+1}^{rad}(R,\omega)W_{-1}(R,\omega)}. \tag{16}$$

Noted that parameter B can be evaluated for each ω directly from the Fourier transformed records. This result is formally as simple as the standard SPAC for vertical records (Aki 1957) since only a finite number of calculations with the waveforms (apart from the ideally continuous azimuthal weighted averaging) are required in order to remove the effects of *Rayleigh* waves. In the case of infinite number of stations on the circular array, phases coming from the Fourier series coefficients cancel out during the computation of B via Eq. (16), providing a real result. Function $f_1(x)$ is the unity for $x = 0$ and continuous and monotonically decreasing to $x = 3.83$ where it takes an

infinite value as shown in Fig. 2a. That function is one-to-one inside the range $[0 \quad 5.14)$, showing a zero crossing at $x = 1.84$. An explicit expression for x_L^2 may be obtained, for example, for long *Love* wavelengths by means of a Taylor series expansion matching the form $x_L^2 = \sum_{n=1}^{\infty} l_n (B-1)^n$, where l_n are real numbers:

$$x_L^2 \approx -4(B-1) - \frac{2}{3}(B-1)^2 - \frac{1}{18}(B-1)^3 + \frac{1}{540}(B-1)^4 + \ldots \qquad (B \le 1). \tag{17}$$

This series is not applicable for $B > 1$ due to the discontinuity in $f_1(x)$ at $x = 3.83$.

Respectively, a suitable way for the determination of *Rayleigh* wave velocity can be obtained from the Eqs. (11) to (13) and definition (16):

$$g(x_R, B) = \frac{f_0(x_R)}{B(R,\omega)\, f_1(x_R) - 1} = C(R,\omega), \tag{18}$$

where a second relevant quantity, C, has been defined as:

$$C(R,\omega) = \frac{iU_0^{rad}(R,\omega)}{W_0(R,\omega)} \frac{W_{-1}(R,\omega)U_{+1}^{rad}(R,\omega) - W_{+1}(R,\omega)U_{-1}^{rad}(R,\omega)}{U_{-1}^{tg}(R,\omega)U_{+1}^{rad}(R,\omega) + U_{-1}^{rad}(R,\omega)U_{+1}^{tg}(R,\omega)}. \tag{19}$$

Equation (18) shows that the wavefield characteristics $A_R^{V,m}$, $A_R^{H,m}$ (with $m = 0, \pm 1$), A_L^m (with $m = \pm 1$) and the ground property χ cancel out in the calculation of C, so that, it depends on x_R and x_L (or B) only, by means of the function $g(x_R, B)$, which has been plotted in Fig. 2b. Function $g(x_R, B)$ is continuous on the variable x_R either up to 2.40 (first infinity in f_0) when $|B| \leq 1$, or up to the first root of $J_1(x) = 1/B$ in any other case. The *Rayleigh* wave property x_R can be worked out by using an appropriate series expansion in Eq. (18). For example, that with the form: $x_R^2 = \sum_{n=1}^{\infty} r_n(B)\, C^n$, with r_n depending on B being given, for $C > 0$ and $B < 1$, by:

$$x_R^2 = 2(1-B)C - \frac{(1-3B)(1-B)}{2}C^2 + (1-B)\frac{3(1-3B)^2 + (5-62B+93B^2)}{96}C^3 + \ldots \quad (20).$$

3 COMPARISONS WITH THE 3C-SPAC METHOD

The formulation of SCAM for calculation of *Love* wave velocities leads to a simpler mathematical expression in comparison with the 3c-SPAC (Okada & Matsushima 1989), since x_L and x_R could not be obtained in an independent manner from the latter method. As shown, B, C and the target quantities x_L and x_R are related by $B = f_1(x_L)$ and $C = g(x_R, B)$, thus, x_L and x_R can be determined by solving

one-unknown equations in terms of unambiguous measurable physical quantities. Since the former relations are not one-to-one, the final values of x_L and x_R should be eventually selected among a set of possible solutions. Equations (14) and (15) also permit to choose the optimum array size for *Love* wave prospecting independently of the *Rayleigh* wave velocities. On the other hand, 3c-SPAC leads to a couple of relationships (see Appendix A) with the form $C_V = J_0(x_R)$ and $C_{tg} = h(C_{rad}, x_R, x_L)$ corresponding with Eq. (A8) and with the result of elimination of $\Re(\omega)$ from (A1) and (A2), respectively. The former one represents the standard vertical-SPAC method for the calculation of x_R. Since $J_0(x)$ cannot be globally inverted, calculation of the *Love* wave property x_L from the latter equation can not be summarized into a unique self-contained relationship, requiring an additional intermediate selection of root in the

Fig. 3

calculation of x_R from C_V.This point has been illustrated in Fig. 3 by using a synthetic wavefield composed of a randomly selected set of 100 plane surface waves. For clarity, a hypothetical constant *Rayleigh* to *Love* wavelength ratio of 2 (non dispersive wavefield) and fixed *Rayleigh* wave ellipticities corresponding to χ = 1 and χ = 10 have been considered. Amplitudes of the *Love* waves and vertical components of the *Rayleigh* waves were chosen in a common range. Coefficients B, C, C_{tg} and C_V calculated from the synthetic records in a 8-sensor array (with a ninth central station for the

3c-SPAC) have been plotted vs. x_L or x_R (asterisks). These results have been compared with the theoretical relations for an infinite dense array derived from the parameters of the incident wavefield $(x_R, x_L, \Re)$, shown with solid lines in Fig. 3. Functions $g(x_R, B)$, and $h(C_{rad}, J_0^{-1}(C_V), x_L)$ with B, C_{rad} and C_V obtained from the finite array records and $J_0^{-1}(C_V)$ chosen as the smaller value of x_R satisfying Eq. (A8) have been shown in Figs 3b and 3c using circles. Differences between asterisks and circles represent, additive misfits in Eq. (18) or in $C_{tg} = h(C_{rad}, x_R, x_L)$, respectively. In the former case (Fig. 3b), misfits are due to the use of an array with finite number of stations. On the other hand, the criterion for selection of roots leads to mistaken values of x_L in the later case, when x_R is around or larger than 3.83 (Fig. 3c). Errors depend on the power of *Rayleigh* waves in the horizontal component, controlled by χ in Fig. 3c.

An interesting alternative approach for calculation of *Rayleigh* wave phase velocities from vertical records in a single Centerless Circular Array setup (CCA method) has been derived by Cho *et al*. (2004) and Cho *et al*. (2006b). They regard microtremor as a random field stationary in time and space and summarize the technique in equation (7) in the latter paper. A similar expression can be retrieved in our theoretical frame by using equation (5) for calculation of $\left|W_0(R,\omega)/W_1(R,\omega)\right|^2$. Nevertheless, this

ratio equals $J_0^2(x_R)/J_1^2(x_R)$ only if $\left|A_R^{V,0}\right| = \left|A_R^{V,1}\right|$, which is not valid for an arbitrary deterministic wavefield composed of plane *Rayleigh* wavefronts.

4 NUMERICAL TESTS

A systematic evaluation of the performance of the SCAM is a rather complicated issue due to the numerous array and wavefield parameters to be considered even if it is simplified by means of hypothesis as dominance of a single mode or absence of body wave effects. Hereafter, the main reasons leading to biased estimations of phase velocities are investigated by using some particular array and source distributions.

4.1 EFFECTS OF THE DIRECTIONAL ALIASING

The finite number of sensors in any real array setup represents a source of bias in the estimates of B and C and in the phase velocities derived from them. Provided that the circular array is made of N^{stat} evenly distributed sensors with one of them placed at the azimuthal coordinate θ = 0 then, the optimum estimators of the Fourier-Series coefficients $W_m(R,\omega)$, $U_m^{rad}(R,\omega)$ and $U_m^{tg}(R,\omega)$ are

$\hat{X}_m(R,\omega) \equiv \frac{2\pi}{N^{stat}} \sum_{j=1}^{N^{stat}} exp(-imj\Delta\theta) X(R, j\Delta\theta, \omega)$ where $\Delta\theta = 2\pi/N^{stat}$ and X

represents W, U^{rad} or U^{tg}. Cho *et al.* (2006a) show that the bias in $\hat{X}_m(R,\omega)$ equals the sum of the $m+jN^{stat}$ –th order Fourier-Series coefficients $X_m(R,\theta,\omega)$, where $j = \pm1, \pm2, \ldots$, that is to say: $\hat{X}_m(R,\omega) = \sum_{j=-\infty}^{+\infty} X_{m+jN^{stat}}(R,\omega)$. Since quantities $X_{m+jN^{stat}}(R,\omega)$ were calculated in equations (5) to (7), the estimators $\hat{B}$ and $\hat{C}$ can be formed substituting $\hat{X}_m(R,\omega)$ for their counterparts in equations (16) and (19). The results are functions of the wavefield characteristics $A_R^{V,m+jN^{stat}}$, $A_R^{H,m+jN^{stat}}$, $A_L^{n+jN^{stat}}$, k_R and k_L where $m = 0, \pm1$; $n = \pm1$; $j = 0, \pm1, \pm2, \ldots$ The analysis of such expressions of $\hat{B}$ and $\hat{C}$, in general cases, is out of the scope of this article. Nevertheless, a rough estimate for the range of the directional aliasing effects may be obtained by checking the method with a single plane wave coming from different source azimuths. Thus, several numerical tests were performed by varying the plane wave directions from $\varphi = 0$ (that is, pointing to a virtual sensor) to $\varphi = \pi / N^{stat}$. The wavefield was composed by both *Rayleigh* and *Love* components. Several *Rayleigh* to *Love* velocity ratios and amplitude ratios were checked. For example, tests corresponding with the fixed wavefield characteristics $A_R^V = A_L$, $\chi(\omega) = 1$ and $c_R / c_L = 0.5$ have been displayed in Figs. 4 and 5. Equivalence between the N^{stat} and the $2N^{stat}$ sensor arrays holds for the v-SPAC method provided that N^{stat} is an odd number (without taking into account the central station). Nevertheless, such property fails for a wavefield composed by an arbitrary sum of plane waves. It also fails for the

Figs 4&5

SCAM and for the *Love* wave analysis using the 3c-SPAC method, whatever the number of plane waves used.

4.2 BIASES DUE TO THE PRESENCE OF NOISE

The robustness of SCAM method in the presence of uncorrelated noise has been investigated by means of numerical tests. The methodology applied in SESAME (2005) has been adapted to the SCAM and to the 3c-SPAC method. Noise is simulated by means of random relative time shifts introduced into the synthesized records. A single monochromatic plane wave composed by both *Rayleigh* and *Love* components has been used as the three-component wavefield coming from a far source. Then, it was recorded in an 8 sensor virtual circular array. Independent time shifts were chosen for each virtual sensor, matching a zero-mean Gaussian distribution with standard deviation σ_t. Since incoherent noise effects should be reduced by using of suitable mean estimators, a total of 500 complete dataset were constructed by using different sets of random time delays. After testing different ways to solve equations (15) and (18), the mean values of B and $|C|$ were estimated as $\widetilde{B} = \sqrt{\langle |n_B|^2 \rangle / \langle |d_B|^2 \rangle} \langle cos(\Phi_B) \rangle$ and $|\widetilde{C}| = \sqrt{\langle |n_C|^2 \rangle / \langle |d_C|^2 \rangle}$ respectively. Quantities n_B, n_C, d_B, d_C and Φ_B stand for the numerator, denominator and phase angle of B and C on the basis of equations (16) and (19).

Symbol $\langle\cdot\rangle$ stands for the mean of the bracketed quantities along the 500 realizations. Finally, the estimators $\tilde{x}_R$ and $\tilde{x}_L$ were calculated from $\tilde{B}$ and $|\tilde{C}|$ by using a grid search algorithm in equations (15) and (18). Thus, the effects of incoherent noise can be quantified as $|\tilde{x}_R - x_R^0| / x_R^0$ and $|\tilde{x}_L - x_L^0| / x_L^0$ where subscript 0 stands for the zero noise case (σ_t = 0). These ratios depend mainly on σ_t / T (related to the Signal to Noise ratio N/S), x_R and x_L, where *T* is the central period of the signal. Figure 6 shows the misfit due to Gaussian time shifts with standard deviations σ_t up to 20% of *T* in a particular case (see figure caption for further details on the wavefield characteristics). This test was also performed for the 3c-SPAC method by using a ninth central station. As shown, the more serious effects of random noise were found for low values of x_R and x_L, that is, in the ranges with small radius-to-wavelength ratios. Robustness of the SCAM for *Love* waves was comparable to that of the 3c-SPAC method in spite of the smaller total number of sensors. The optimum performance in this case was found approximately for x_L around the first zero-crossing of $f_1(x_L)$ at x_L = 1.84 (Fig. 2c). It coincides also with a minimum in the expression $|f_1(x_L)/(x_L\, df_1(x_L)/dx_L)|$, which roughly represents the magnification of the relative errors from $\tilde{B}$ to $\tilde{x}_L$:

Fig. 6

$$\frac{variance(\tilde{x}_L)}{\tilde{x}_L^2} \approx \left| \frac{f_1(x_L)}{x_L \, df_1(x_L)/dx_L} \right|^2 \frac{variance(\tilde{B})}{\tilde{B}^2}. \qquad (21).$$

Finally, we note that robustness of the SCAM for *Rayleigh* waves is worse than that for the 3c-SPAC method in some ranges of interest, for expample x_R around 1 and σ_t around 5 % of *T*.

4.3 NUMERICAL TESTS IN A 1D LAYERED MEDIUM

Finally, the SCAM has been studied and compared with the 3c- SPAC method in a more realistic synthetic microtremor wavefield, generated by a random distribution of point sources applied on the free surface of a layered 1D ground structure. Two different array setups made up of 9 virtual sensors were used in the tests (shapes in Fig. 7). If effects of the body waves are neglected, the time histories recorded at any station of the array due to a harmonic point force can be calculated (see Appendix C) from the elastodynamic parameters of the ground (*S*-wave velocity V_{Si}, *P*-wave velocity V_{Pi}, mass density ρ_i, Table 1 and thickness H_i, where *i* identifies the layer, see Fig 10). A simple soil structure (Table 1), consisting of a single 100 m thick soft layer overlying a stiffer halfspace, has been used for this test. Array radius was fixed to *R* = *H*. It can be considered a suitable

choice for the exploration of depths around the layer interface in case of the standard vertical-component SPAC although, in practice, the surveyed depth range is also limited by the source excitation spectrum and the high pass filtering effect of the upper soft layers (e. g. Scherbaum *et al*. 2003). A set of 1000 impulsive point sources randomly distributed with distances from the center of the array raging between 3R and 10R has been used for the simulation of the microtremor wavefield (Fig. 7a). Records synthesized at the center of the array have been shown in Fig 7b. Origin times were randomly selected for each point source in an appropriate range permitting the signals spreading with the maximal and minimal group velocities to reach the array position from t = 0 sec to t = 550 sec. The maximum frequency considered in the former step was 4.1 Hz. Point forces were generated with arbitrary directions whereas their amplitudes were randomly chosen in a predetermined range following a uniform probability distribution. Signals were subsequently convolved in frequency domain with 10 Hanning windows centered from t = 50 sec to 500 sec with a 100 sec width and 50 % overlapping.

Fig. 7

Hereafter, the synthetic microtremor records are analyzed on the basis of equations (15) and (18). Several slightly different numerical schemes can be used for this task. Although this is maybe not the optimum choice in terms of robustness of the solutions, phase velocities were independently calculated for each time window. In this

way, the stability of the final velocity estimations can be checked. Quantities B and C in the aforementioned equations were replaced with the real parts of their values derived from the records by means of equations (16) and (19).

The averaged B and C coefficients have been shown in Figs. 7c and 7d respectively. Phase velocities of *Rayleigh* and *Love* waves were bracketed by applying a grid-search method in the slowness-frequency domain to equations (15) and (18). A grayscaled image representing the number of solutions found inside each cell for the whole window set has been drawn (Figs 7e and 7f). As shown, effects of finite window length and near sources are enlarged by the flat shapes of functions $f_1(x_L)$ and $g(x_R, B)$ in the low frequency range (see also Fig. 3c). As well, effects of spatial aliasing and/or non-uniqueness of solutions (inside the velocity range shown) become noticeable above 2.9 Hz for *Love* waves and 2.2 Hz for *Rayleigh* waves. Thus, the array size should be reduced or the number of sensors increased in order to improve the curves in that frequency band. Generally, the former option would be more suitable since shapes of $f_1(x_L)$ and $g(x_R, B)$ are simpler as x_L and x_R are smaller. The application of the 3c-SPAC method (Appendix A) for the synthetic dataset recorded with the 3c-SPAC array

Fig. 8

setup (Fig. 7a) has been shown in Fig. 8. In this case, equations (15) and (18) are replaced with $C_{tg} = h(C_{rad}, x_R, x_L)$ and $C_V = J_0(x_R)$ as described in the previous section.

Details regarding time-window generation and search for solutions were the same as for the SCAM. First, all possible solutions for x_R within the considered slowness range were calculated for each frequency by solving $C_V = J_0(x_R)$. Then, these solutions were introduced into the former equation for the calculation of the corresponding set of roots for x_L. Figs. 7f and 8e show that accuracy on the determinations of *Rayleigh* wave velocities from Aki's method, which takes full advantage of the cancellation of *Love* waves in the vertical component, is slightly better than for the proposed scheme, mainly in the low frequency band. On the other hand, the SCAM supplied very accurate results for the *Love* wave dispersion curve, with some improvement in the high frequency range due to the absence of nearby solutions for Eq. (15) and to the higher azimuthal sampling achieved by moving the central sensor to the circumference (Figs. 7e and 8d).

A second numerical experiment was carried out by relaxing the far-source constraint in such a manner that only the area enclosed by the array is maintained free of

Fig. 9

sources (Figs. 7a and 9). Note that such scenarios were not considered in the formulation of this method, thus, biased results are to be expected a priori. The comparison of dispersion curves confirms that their quality gets increasingly worse, mainly in the lower frequency band if sources are permitted close to the array. Thus, general recommendations regarding minimization of near sources in microtremor array

techniques (i. e, SESAME 2005) are equivalently valid for the SCAM.

5 CONCLUSIONS

We have described in this paper the foundations of a new technique aimed at the determination of ground structures from three-component array analysis. The proposed Single Circular Array Method (SCAM) is useful for the calculation of *Rayleigh* and *Love* wave dispersion curves in wavefields generated by any number of sources. This is done by using an array setup consisting of a circular arrangement of sensors without a central device. Since *Rayleigh* and *Love* wave velocities show different sensitivities to the elastodynamic parameters that characterize the medium, the SCAM can be used to obtain better constrained ground models in comparison with methods only based on the vertical component. In comparison with the 3c-SPAC method, the SCAM provides a rather straightforward way for the calculation of *Love* wave phase velocities.

Most of the spatial autocorrelation methods rest on the theoretical frame of stochastic processes, on the hypothesis of independence among *Love* and *Rayleigh* waves, and/or on the independence among waves coming from different directions. On the contrary, the SCAM follows a deterministic approach and remains valid even if plane waves are mutually correlated, in the sense of Cho *et al.* (2006a).

Horizontal and vertical component records need to be obtained simultaneously for the SCAM, while vertical components can be recorded in a separate experiment for the 3c-SPAC method. Irrelevance of the records at the centre of the circular array is a favorable feature of the new method in some geological contexts.

Reliability of this method has been validated by numerical tests. Studies using a synthetic dataset of microtremor records show good performance for univocal retrieval of *Love* wave dispersion curves up to a larger radius to wavelength ratio, in comparison with other array methods. In order to check the robustness of the method, uncorrelated noise was added to a synthetic surface wavefield. The analysis of that dataset showed that robustness of the SCAM is similar to that of the 3c-SPAC method for *Love* wave analysis, and is optimized around x_L = 1.84, approximately (for a *Love* wavelength to radius ratio around 3.4). In the case of *Rayleigh* waves, the 3c-SPAC method seems to be less sensitive to uncorrelated noise. Nevertheless, further studies are necessary in order to assess these conclusions in different conditions of the wavefield.

A second synthetic dataset composed of cylindrical surface waves generated by a distribution of sources acting on the free surface of a realistic structure has been analyzed. Results seems to confirm that the maximum performance of the SCAM for *Love* waves occurs in a wide range around the first zero crossing of B (x_L = 1.84). The

absence of sources in the vicinity of the array leads to a significant improvement on dispersion curve estimates.

Finally, we provide some issues that should be considered when using the SCAM in practice:

i) Equations of the SCAM have been derived assuming that *Rayleigh* wavefield is dominated by single mode which is the same in both vertical and horizontal components. Dominance of a single *Love* mode was admitted too.

ii) The relative power of body waves in the wavefield should be negligible in order to apply any of the aforementioned methods. Generally, this hypothesis holds in most of the frequency bands provided that the sources are far enough from the array (Tokimatsu 1997). The dominance of surface waves in microtremor has been also checked in experimental studies (i. e. Chavez-García & Luzón 2005).

iii) The power of the microtremor wavefield should be large enough in the frequency band of interest to guarantee a suitable signal to noise ratio. Such power depends on the source excitation spectra and on the filter effects of the geological structure. In particular, suitable vertical component records are required to separate *Love* and *Rayleigh* waves in the horizontal components.

Thus, performances of both the SCAM and the 3c-SPAC fail if *Rayleigh* waves degenerates into pure horizontal motion.

iv) The SCAM and the CCA method for *Rayleigh* wave analysis can be used together since the array setup is same. Note that the particular hypothesis of CCA method should be satisfied too.

ACKNOWLEDGEMENTS

The authors gratefully thank the Editor, Dr. Ikuo Cho and an anonymous referee for their constructive comments which significantly improved this article. We especially thank Dr. M. Santoyo for the careful reading of this manuscript. This research was supported by the Spanish CICYT projects REN2003-08159-C02-01, CGL2005-05500-C02-02/BTE, CGL2007-66745-C02-02/BTE, the FPI program of the Spanish Ministry of Education and Science and the European Community with European Social Funds and FEDER. We used resources owned by the Geofísica Aplicada team RNM194 of Junta de Andalucía, Spain.

REFERENCES

Abramowitz, M. & Stegun I. A., 1972. *Handbook of mathematical functions,* Dover, New York.

Aki, K., 1957. Space and time spectra of stationary stochastic waves, with special reference to microtremors, *Bulletin of the Earthquake Research Institute,* 35, 415–456.

Arai, H., Tokimatsu, K., 2005. S-Wave Velocity Profiling by Joint Inversion of Microtremor Dispersión Curve and Horizontal-to-Vertical (H/V) Spectrum, *Bull. Seism. Soc. Am.*, 95(5), 1766–1778.

Chávez-García, F.J., & Luzón, F., 2005. On the correlation of the seismic microtremors. *J. Geophys. Res.* 110, doi: 10.1029/2005JB003671.

Cho, I., Tada, T. & Shinozaki, Y., 2004. A new method to determine phase velocities of Rayleigh waves from microseisms, *Geophysics*, 69, 1535– 1551.

Cho, I., Tada, T. & Shinozaki, Y., 2006a. A generic formulation for microtremor exploration methods using three-component records from a circular array, *Geophys. J. Int.*, 165, 236-258.

Cho, I., Tada, T. & Shinozaki, Y., 2006b. Centerless circular array method: Inferring phase velocities of Rayleigh waves in broad wavelength ranges using microtremor records, *J. Geophys. Res*., 111, B09315, doi:10.1029/2005JB004235.

García-Jerez, A., Luzón, F. & Navarro, M., 2006a. Computation of dispersion curves for Rayleigh and Love waves using horizontal components of seismic microtremor, *8th U.S. National Conference on Earthquake Engineering, San Francisco, USA, April 2006*, paper N. 1377.

García-Jerez, A., Luzón, F. & Navarro, M., 2006b. Cálculo de características de las ondas superficiales usando ruido ambiental mediante medidas de array de tres componentes, *5ª Asamblea Hispano-portuguesa de Geodesia y Geofísica, February 2006, Sevilla, Spain*.

García-Jerez, A., Luzón, F., Navarro, M. & Pérez-Ruiz, J. A., 2008. Determination of elastic properties of shallow sedimentary deposits applying a spatial autocorrelation method, *Geomorphology,* 93, 74-78.

Harkrider, D. G., 1963. Rayleigh and Love waves from sources in a multilayered elastic half-space, Ph.D. thesis, California Institute of Technology, Pasadena, Calif.

Harkrider, D. G., 1964. Surface waves in multilayered elastic media; I, Rayleigh and Love waves from buried sources in a multilayered elastic half-space, *Bull. Seism. Soc. Am.*, 54(2), 627-679.

Haskell, N. A., 1953. The dispersion of surface waves on multilayered media, *Bull. Seism. Soc. Am*., 43, 17-34.

Henstridge, J. D., 1979. A signal processing method for circular arrays, *Geophysics*, 44,

179-184.

Köhler, A., Ohrnberger, M., Scherbaum, F., Wathelet, M. & Cornou, C., 2007. Assessing the reliability of the modified three-component spatial autocorrelation technique, *Geophys. J. Int.*, 168(2), 779-796.

Métaxian, J-P. & Lesage, P. J., 1997. Permanent tremor of Masaya Volcano, Nicaragua: Wave field analysis and source location, *J. Geophys. Res.*, 102, 22529-22545.

Morikawa, H., 2006. A method to estimate phase velocities of surface waves using array observations records of three-component microtremors, *Structural Eng. / Earthquake Eng., JSCE,* 23, 143s – 148s.

Noguchi, T. & Nishida, R., 2002. Determination of Subsurface Structure of Tottori Plain Using Microtremors and Gravity Anomaly, *Journal of Natural Disaster Science,* 24(1), 1-13.

Okada, H., 2006. Theory of efficient array observations of microtremors with special reference to the SPAC method, *Exploration Geophysics*, 37, 73-85.

Okada, H. & Matsushima, T., 1989. An exploration Technique using microtremors (1) – an analytical background to discriminate Love wave in microtremors –, *81st Annual Meeting for Society of Exploration Geophysicist of Japan, Japan.*

Parolai, S., Picozzi, M., Richwalski, S. M. & Milkereit, C. 2005. Joint inversion of phase

velocity dispersion and H/V ratio curves from seismic noise recordings using a genetic algorithm, considering higher modes, *Geophys. Res. Lett.*, 32, L01303, doi:10.1029/2004GL021115.

Sakai, K., & Morikawa, H., 2006. A method to estimate 2-D subsurface structure using gravity and microtremor data and its application, *3rd International Symposium on the Effects of Surface Geology on Seismic Motion, Grenoble, France, August 2006*.

Scherbaum, F., Hinzen, K. G. & Ohrnberger, M. 2003. Determination of shallow shear wave velocity profiles in the Cologne, Germany area using ambient vibrations, *Geophys. J. Int.*, 152, 597-612.

SESAME, 2005, Report on FK/SPAC Capabilities and Limitations, WP06 - Derivation of dispersion curves, *SESAME-Project, EVG1-CT-2000-00026*, Report-Nr.: D19.06, http://sesame-fp5.obs.ujf-grenoble.fr

Tokimatsu, K., 1997. Geotechnical site characterization using surface waves, *in Earthquake Geotechnical Engineering*, pp. 1333-1368, ed. Ishihara, Balkema, Rótterdam.

Wathelet, M., 2005. *Array recordings of ambient vibrations: surface-wave inversion*, PhD thesis, University of Liège, Belgium.

FIGURE CAPTIONS

Figure 1. Sketch of the array setup used in the proposed microtremor surveying method. Cylindrical coordinates defining station positions and surface plane wave directions.

Figure 2. (a) Shapes of functions $f_0(x)$ and $f_1(x)$. (b) Shape of the function $g(x_R, B)$. (c) Shape of the functions $1/\left|df_1(x)/dx\right|$ and $\left|f_1(x)/(x\, df_1(x)/dx)\right|$.

Figure 3. B vs. x_L (panel a), C vs. x_R (panel b), C_{tg} vs. x_L (panel c) and C_V vs. x_R (panel d) relations calculated for a randomly generated wavefield in a 8 – sensor circular array. Wavefield consists of 50 plane *Rayleigh* waves and 50 plane *Love* waves. A *Rayleigh* to *Love* wavelength ratio of 2 and ellipticities corresponding to χ = 1 and χ = 10 have been fixed for clarity (see text). Asterisks show coefficients calculated from the synthetic records. Theoretical relations for a continuous array calculated from the wavefield characteristics (k_R, k_L and $\Re$) have been shown with solid lines. Functions $g(x_R, B)$ and $h(C_{rad}, J_0^{-1}(C_V), x_L)$ evaluated by using B, C_{rad} and C_V obtained from the synthetic records have been drawn with circles in panels b and c (see text). Vertical dashed lines in panel c show the value of x_L corresponding with x_R = *3.83*. Only real parts are shown for complex quantities.

Figure 4. $\hat{B}$ vs. x_L and $\hat{C}$ vs. x_R calculated by using a circular array made of N^{stat} evenly distributed virtual sensors. Wavefield consists of a single plane wave traveling to

the azimuthal coordinates φ = 0, $\pi/(3\ N^{stat})$, $2\pi/(3\ N^{stat})$ or $\pi/\ N^{stat}$ with x_R/x_L = 0.5, χ =1 and $A_R^V = A_L = 1$.

Figure 5. Deviations in x_L and x_R calculated for an N^{stat} – sensor virtual array (asterisked) regarding to their actual values. The lines are computed from the cases shown in Fig. 4 and using the same type of lines.

Figure 6. Misfits on x_L (panels a and c) and x_R (panels b and d) due to incoherent noise effects obtained by using the SCAM (a and b) and the 3c-SPAC method (c and d). Quantity σ_t represents the variance of the Gaussian time shifts used for the simulation of noise. Wavefield was composed by a single monochromatic plane wave with both *Rayleigh* and *Love* components traveling to the azimuthal coordinate φ = $\pi/32$ with x_R/x_L = 0.5, χ =1 and $A_R^V = A_L$ =1. An 8-sensor virtual array with an additional central station for the 3c-SPAC method has been used. Symbol ~ and subscript 0 refer to “noisy records” and “zero noise records”, respectively.

Figure 7. (a) Distribution of random sources (dots) generating the simulated microtremor wavefield with distances up to *1km* from the center of the nine-sensor array. Positions of stations have been shown with triangles. The array setup used for the 3c-SPAC method (Fig. 8) is shown in the top left corner. Sources inside the arrays were not considered in the wavefield calculations. The *3R* distance has been indicated with a solid line. (b)

Synthetic microtremor records at the center of the array. (c) B coefficient (circles) calculated from synthetic array records. Solid line shows $f_1(x_L)$ computed from the theoretical *Love* wave velocities. (d) C coefficient computed from synthetic array records. (e) Solutions for *Love* wave phase dispersion curve calculated from $B(\omega)$. Grayscale shows the stability of the solutions along the time-window set. Actual dispersion curve is shown with a dashed line. (f) *Rayleigh* wave phase dispersion curve (grayscaled zones) calculated from both $B(\omega)$ and $C(\omega)$ coefficients. Theoretical curve is drawn using a dashed line. The actual resolution in frequency is 0.01 Hz Nevertheless, quantities $B(\omega)$ and $C(\omega)$ have been shown for some frequencies only in sake of clarity.

Figure 8. (a) Radial correlation coefficient C_{rad} obtained from synthetic microtremor records. (b) Tangential correlation coefficient C_{tg}. (c) Vertical-component correlation coefficient C_V. That calculated from theoretical dispersion curve is shown with a solid line. (d) *Love* wave phase dispersion curve calculated from $C_V(\omega)$, $C_{rad}(\omega)$ and $C_{tg}(\omega)$ by using 3c-SPAC (grayscale). Theoretical curve is shown with a dashed line. (e) *Rayleigh* wave phase dispersion curve calculated from $C_V(\omega)$ and theoretical curve. Correlation coefficients have been shown for some frequencies only in sake of clarity.

Figure 9. Comparison among *Love* (left hand side plots) and *Rayleigh* (right hand side plots) wave dispersion curves, obtained by means of the 3c-SPAC (bottom) and the

SCAM (top), with and without near sources. Distribution of sources is shown in Fig. 7a. Results considering sources with distances from the array center larger than R are shown with triangles. Those for distances larger than $3R$ are shown using dots. Solid lines show curves computed directly with the ground model. Correlation coefficients have been shown for some frequencies only in sake of clarity.

Figure 10. Source and array coordinate systems and elastodynamic parameters defining a 1D layered ground structure. V_{Si}, V_{Pi}, ρ_i and H_i stand for *S*-wave velocity, *P*-wave velocity, mass density and thickness of the *i*-th layer.

TABLES

Table 1. One-dimensional ground model for microtremor wavefield simulation.

N. Layer	V_S (m / sec)	V_P (m / sec)	H (m)	ρ (g/cm^3)
1	500	935	100	2.1
2	1000	1870	∞	2.1

FIGURES

Figure 1.

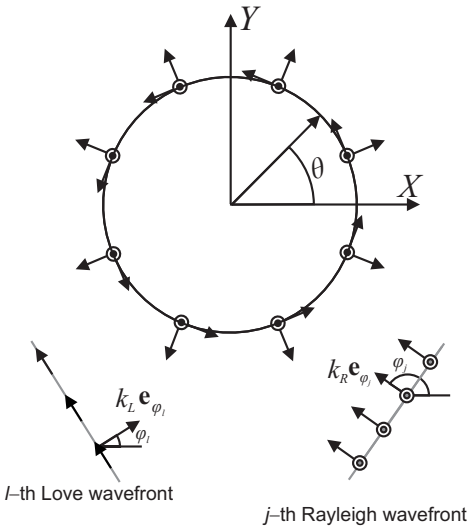

Figure 2.

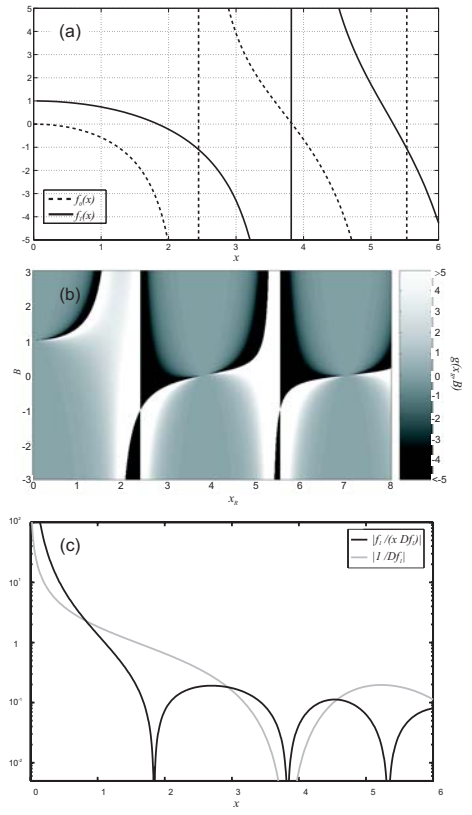

Figure 3

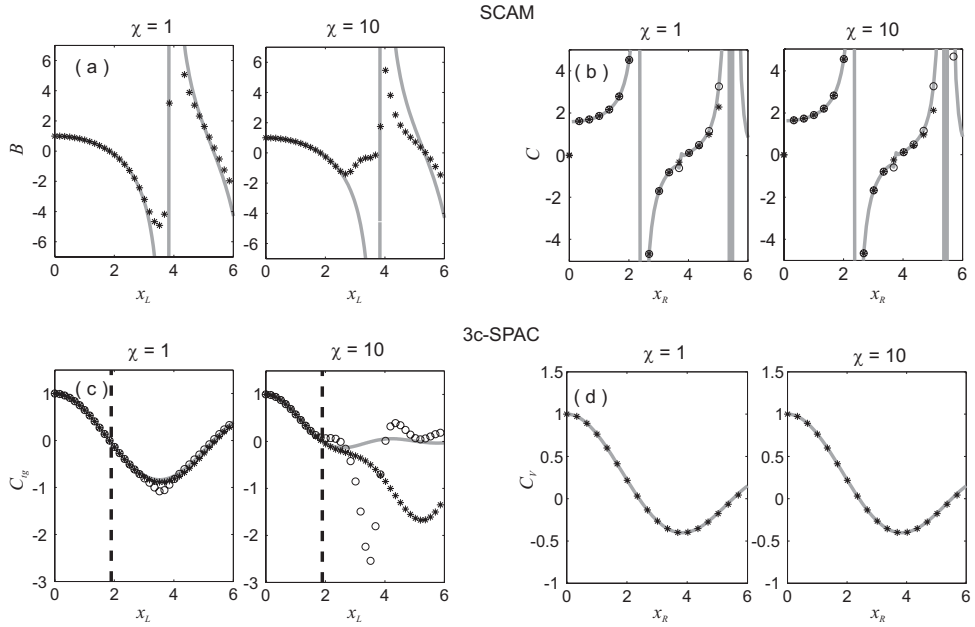

Figure 4

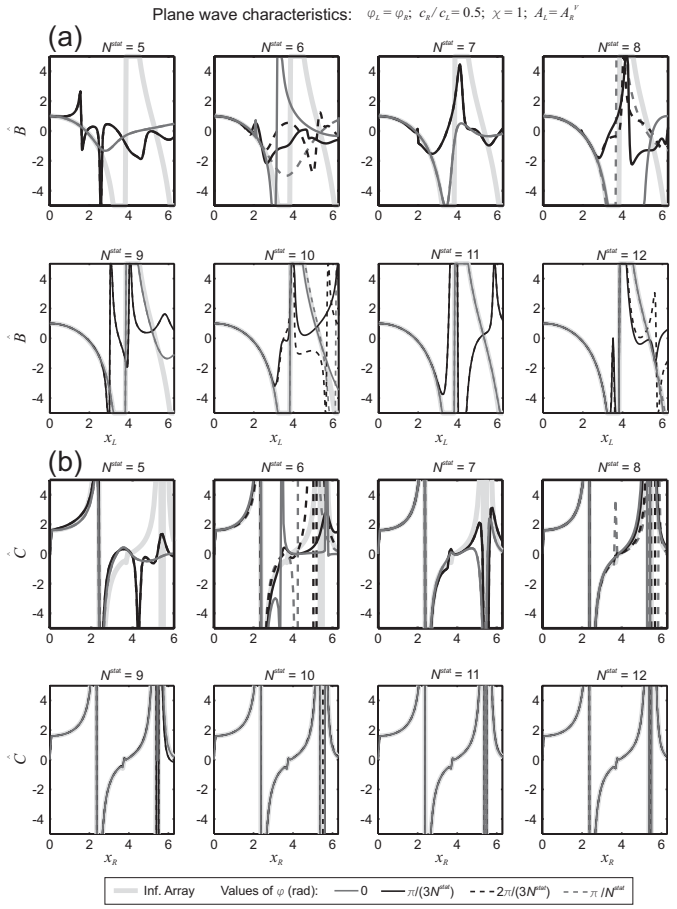

Figure 5

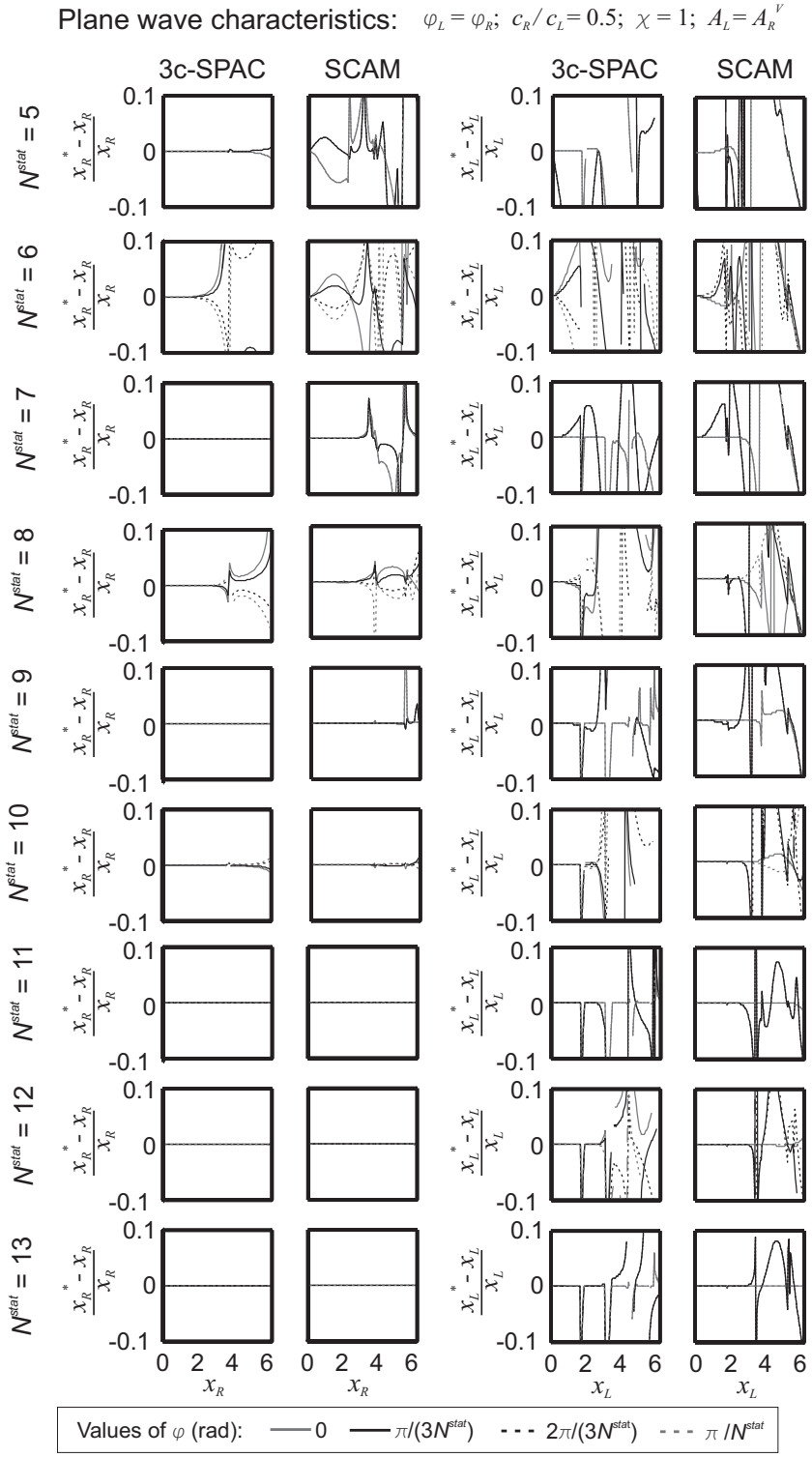
Plane wave characteristics: $\varphi_L = \varphi_R$; $c_R / c_L = 0.5$; $\chi = 1$; $A_L = A_R^{\nu}$
3c-SPAC
SCAM
3c-SPAC
SCAM
N^{stat} = 5
N^{stat} = 6
N^{stat} = 7
N^{stat} = 8
N^{stat} = 9
N^{stat} = 10
N^{stat} = 11
N^{stat} = 12
N^{stat} = 13
$\frac{x_R^* - x_R}{x_R}$
$\frac{x_L^* - x_L}{x_L}$
0.1
0
-0.1
0 2 4 6
x_R
x_L
Values of φ (rad): 0 $\pi/(3N^{stat})$ $2\pi/(3N^{stat})$ π/N^{stat}

Figure 6

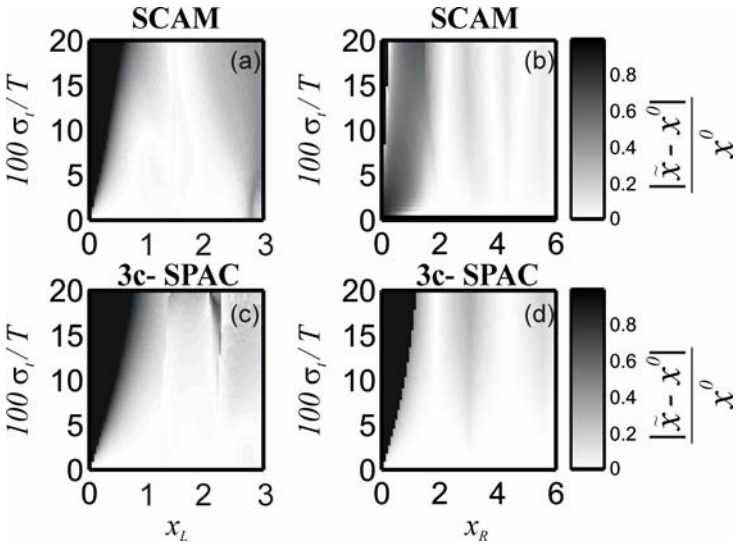

Figure 7

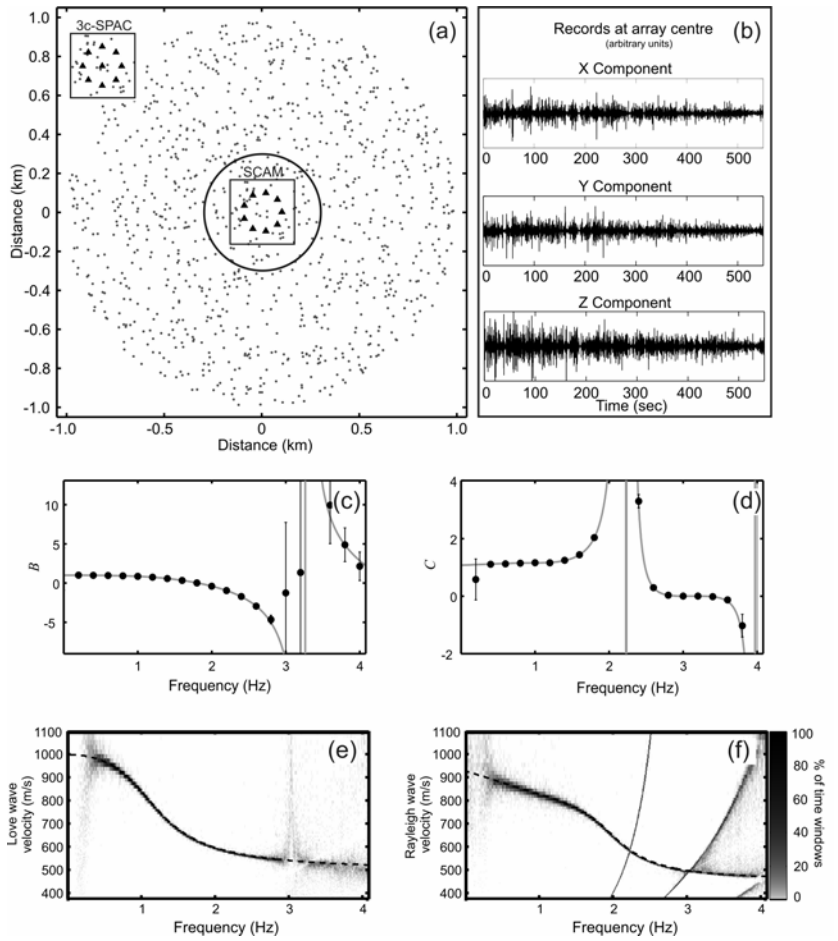

Figure 8

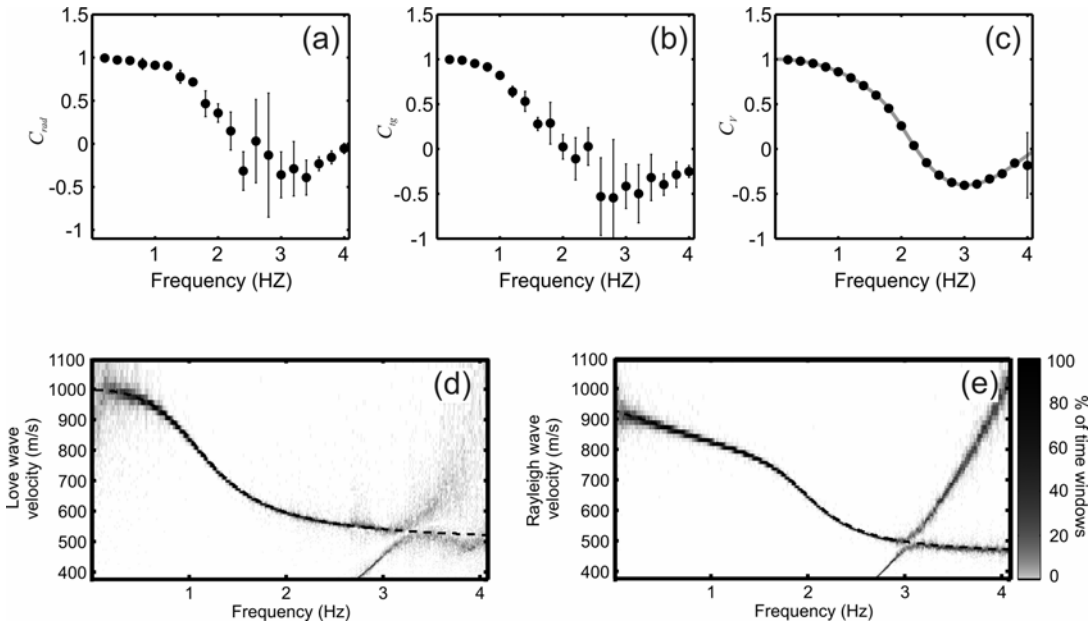

Figure 9

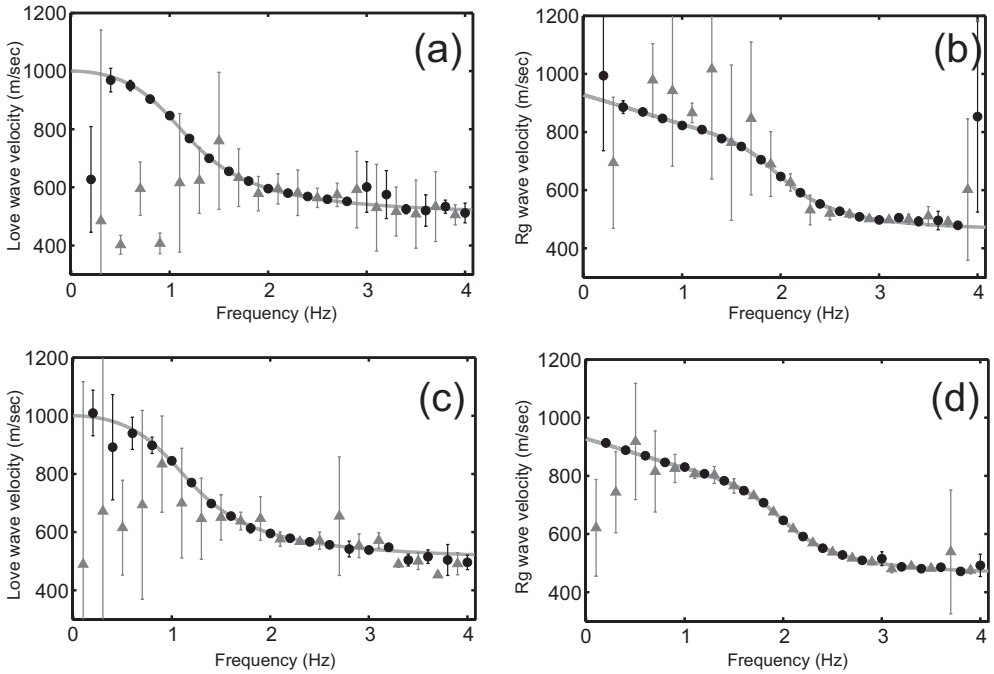

Figure 10

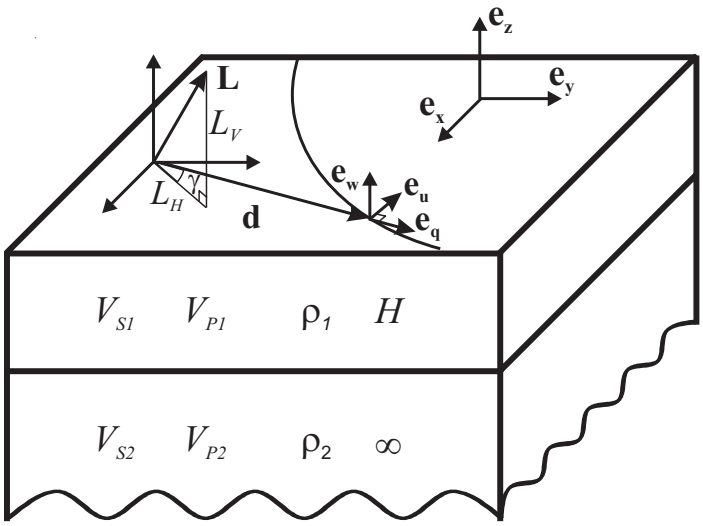

APPENDIX A: THE 3C-SPAC METHOD FOR A WAVEFIELD COMPOSED OF A SUPERPOSITION OF PLANE SURFACE WAVE ARRIVALS

The 3-component SPAC method for derivation of *Rayleigh* and *Love* wave dispersion curves from microtremor measurements recorded on a circular array with central station was established by Aki (1957) and Okada & Matsushima (1989). A review with a detailed mathematical derivation has been recently published by Morikawa (2006). This method can be directly adapted to the hypothesis and representation of the wavefield presented in Eq. (1). Thus, the wavefield will no longer be considered as a stationary stochastic process. Independence among *Rayleigh* and *Love* waves will also be given up, contrary to the original derivation. Thus, Eqs. (24) and (25) in Morikawa's article can be rewritten here as:

$$C_{rad}(\omega) = \left(J_0(x_R) - J_2(x_R)\right)\Re(\omega) + \left(J_0(x_L) + J_2(x_L)\right)(1 - \Re(\omega)), \quad \text{(A1)}$$

$$C_{tg}(\omega) = \left(J_0(x_R) + J_2(x_R)\right)\Re(\omega) + \left(J_0(x_L) - J_2(x_L)\right)(1 - \Re(\omega)), \quad \text{(A2)}$$

where $J_n(x)$ represents the n - order Bessel function and $C_{rad} = \overline{S}_{rad}(R,\omega)/\overline{S}_{rad}(0,\omega)$ and $C_{tg} = \overline{S}_{tg}(R,\omega)/\overline{S}_{tg}(0,\omega)$ stand for the normalized

azimuthally averaged cross-correlations between radial and tangential records at the central station and those on the circumference. Thus, $\overline{S}_{rad}(R,\omega)$ and $\overline{S}_{tg}(R,\omega)$ should be defined as:

$$\overline{S}_{rad}(R,\omega) = \int_{-\pi}^{\pi} U^{rad*}(0,\theta,\omega) U^{rad}(R,\theta,\omega) d\theta, \qquad \text{(A3)}$$

$$\overline{S}_{tg}(R,\omega) = \int_{-\pi}^{\pi} U^{tg*}(0,\theta,\omega) U^{tg}(R,\theta,\omega) d\theta, \qquad \text{(A4)}$$

where asterisks denote complex conjugation. Quantities $U^{rad}(0,\theta,\omega)$ and $U^{tg}(0,\theta,\omega)$ can be expressed in terms of combinations of the weighted amplitudes $A_R^{H,\pm 1}$, $A_L^{\pm 1}$ (defined in Eqs. (8-10)) and $exp(\pm i\theta)$ factors:

$$U_{rad}(0,\theta,\omega) = \frac{(A_R^{H,+1} - iA_L^{+1})}{2} exp(i\theta) + \frac{(A_R^{H,-1} + iA_L^{-1})}{2} exp(-i\theta), \qquad \text{(A5)}$$

$$U_{tg}(0,\theta,\omega) = \frac{(iA_R^{H,+1} + A_L^{+1})}{2} exp(i\theta) + \frac{(-iA_R^{H,-1} + A_L^{-1})}{2} exp(-i\theta) \qquad \text{(A6)}$$

Thus, the integrals (A3) and (A4) can be directly connected with $U_{\pm 1}^{rad}(\omega,R)$

and $U_{\pm 1}^{tg}(\omega,R)$ by using their definitions, and finally, written in terms of Bessel functions on x_R and x_L and of $A_R^{H,\pm 1}$, $A_L^{\pm 1}$ coefficients by means of Eqs. (6) and (7). The results are Eqs. (A1) and (A2), with $\Re$ given by:

$$\Re = \frac{\left|A_R^{H,+1}\right|^2 + \left|A_R^{H,-1}\right|^2 + i\left(A_R^{H,+1}A_L^{+1*} - A_R^{H,-1}A_L^{-1*}\right)}{\left|A_R^{H,+1}\right|^2 + \left|A_R^{H,-1}\right|^2 + \left|A_L^{+1}\right|^2 + \left|A_L^{-1}\right|^2 - 2\,Im\left(A_R^{H,+1}A_L^{+1*} - A_R^{H,-1}A_L^{-1*}\right)} \qquad \text{(A7)}$$

Function $\Re(\omega)$ is named "power ratio of *Rayleigh* waves" since these waves represent the only contribution if $\Re = 1$, while (A1) and (A2) depend only on the *Love* wave characteristics if $\Re = 0$. Note that $\Re$ is not a real quantity unless $Re\left(A_R^{H,+1}A_L^{+1*}\right) = Re\left(A_R^{H,-1}A_L^{-1*}\right)$. Both x_L and $\Re$ can be derived from (A1) and (A2) if x_R is supplied from the usual vertical SPAC method (Aki 1957):

$$C_V = \overline{S}_V(R,\omega)/\overline{S}_V(0,\omega) = J_0(x_R), \qquad \text{(A8)}$$

where $\overline{S}_V(R,\omega) = \int_{-\pi}^{\pi} W^*(0,\theta,\omega)W(R,\theta,\omega)d\theta$, which can be derived from Eq. (5) for $m = 0$.

APPENDIX B: DERIVATION OF EQUATIONS (11) TO (13)

Equations (11), (12) and (13) can be derived if quantities depending on the plane wave amplitudes are eliminated among the equations (4), (5), (6) and (7). Among the infinite set of possibilities, that involving the smallest values of m (in absolute value) was chosen. The forms of equations (5) for $m = 0$ and $m = \pm 1$ are:

$$W_0(R,\omega) = 2\pi A_R^{V,0} J_0(x_R) \quad \text{and} \tag{B1}$$

$$W_{\pm 1}(R,\omega) = -2\pi i A_R^{V,\pm 1} J_1(x_R), \tag{B2}$$

respectively. In the same way, equation (6) yields

$$U_0^{rad}(R,\omega) = -2\pi i A_R^{H,0} J_1(x_R) \quad \text{and} \tag{B3}$$

$$U_{\pm 1}^{rad}(R,\omega) = \pi A_R^{H,\pm 1}\left(J_0(x_R) - J_2(x_R)\right) \mp i\pi A_L^{\pm 1}\left(J_0(x_L) + J_2(x_L)\right). \tag{B4}$$

On the other hand, equation (7) is required for $m = \pm 1$ only:

$$U_{\pm 1}^{tg}(R,\omega) = \pm i\pi A_R^{H,\pm 1}\left(J_0(x_R) + J_2(x_R)\right) + \pi A_L^{\pm 1}\left(J_0(x_L) - J_2(x_L)\right) \qquad \text{(B5)}$$

Dividing (B3) by (B1) and using equation (4) in the form $A_R^{H,0}(\omega)/A_R^{V,0}(\omega) = -i\chi(\omega)$ we obtain:

$$U_0^{rad}(R,\omega)/W_0(R,\omega) = -\chi J_1(x_R)/J_0(x_R), \qquad \text{(B6)}$$

which corresponds to equation (11) once definition (14) is introduced.

For deviation of (12) and (13), quantities $A_L^{\pm 1}$ must be eliminated from equations (B4) and (B5). After some algebra, it yields:

$$U_{\pm 1}^{rad}(R,\omega) f_1(x_L) \pm i U_{\pm 1}^{tg}(R,\omega) = \pi A_R^{H,\pm 1} \frac{2J_1(x_R)}{x_R}\left[f_1(x_R) f_1(x_L) - 1\right], \qquad \text{(B7)}$$

where the relation $\left(J_0(x) + J_2(x)\right) = 2J_1(x)/x$ and the definition (14) have been used. Finally, if equation (B7) is divided by (B2), and the ratio $A_R^{H,\pm 1}(\omega)/A_R^{V,\pm 1}(\omega)$ is subsequently replaced with $-i\chi(\omega)$ (from equation 4) then, the expression

$$\frac{U_{\pm 1}^{rad}(R,\omega) f_1(x_L) \pm i U_{\pm 1}^{tg}(R,\omega)}{\left[f_1(x_R) f_1(x_L) - 1\right] W_{\pm 1}(R,\omega)} = \frac{\chi(\omega)}{x_R}, \qquad \text{(B8)}$$

arises. It corresponds to both equation (12) (upper signs) and equation (13) (lower signs).

APPENDIX C: SURFACE WAVEFIELD DUE TO AN HARMONIC SHALLOW POINT SOURCE

The surface wavefield generated by a harmonic point source with horizontal component L_H and vertical component L_V applied on the free surface of a layered 1D ground structure can be calculated as the sum of the contributions corresponding to the *Rayleigh* and *Love* normal modes:

$$w_S = \sum_m \left[w_{R_m}^H + w_{R_m}^V \right], \quad q_S = \sum_m \left[q_{R_m}^H + q_{R_m}^V + q_{L_m}^H \right], \quad u_S = \sum_m \left[u_{R_m}^H + u_{L_m}^H \right], \tag{C1}$$

where w_S, q_S and u_S represent the vertical, radial and tangential displacements at the receiver coordinates, respectively (Fig. 10). The superscript (*H* or *V*) refers to the source component generating each term. The subscripts *R* and *L* correspond to *Rayleigh* and *Love* waves respectively while *S* stands for "surface waves". The value of each contribution was computed by Harkrider (1963 and 1964) as:

Fig. 10

$$w_{R_m}^V(\omega) = L_V(\omega)\Gamma_{Rm}^{V,V}(\omega)H_0^{(2)}(k_{Rm}d), \tag{C2}$$

$$q_{R_m}^V(\omega) = L_V(\omega)\Gamma_{Rm}^{V,H}(\omega)H_1^{(2)}(k_{Rm}d), \tag{C3}$$

$$w_{R_m}^{H}(\omega) = L_H(\omega)\Gamma_{Rm}^{H,V}(\omega)H_1^{(2)}(k_{Rm}d)\cos\gamma\,, \tag{C4}$$

$$q_{R_m}^{H}(\omega) = L_H(\omega)\Gamma_{Rm}^{H,H}(\omega)\left[\frac{H_1^{(2)}(k_{Rm}d)}{k_{Rm}d} - H_0^{(2)}(k_{Rm}d)\right]\cos\gamma\,, \tag{C5}$$

$$u_{R_m}^{H}(\omega) = L_H(\omega)\Gamma_{Rm}^{H,H}(\omega)\frac{H_1^{(2)}(k_{Rm}d)}{k_{Rm}d}\sin\gamma\,, \tag{C6}$$

$$u_{L_m}^{H}(\omega) = L_H(\omega)\Gamma_{Lm}(\omega)\left[\frac{H_1^{(2)}(k_{Lm}d)}{k_{Lm}d} - H_0^{(2)}(k_{Lm}d)\right]\sin\gamma\,, \tag{C7}$$

$$q_{L_m}^{H}(\omega) = L_H(\omega)\Gamma_{Lm}(\omega)\frac{H_1^{(2)}(k_{Lm}d)}{k_{Lm}d}\cos\gamma\,, \tag{C8}$$

where Γ symbols depend on the *Rayleigh* and *Love* medium responses and ellipticities of the surface wave modes ($\chi_m(\omega)$), satisfying $\Gamma_{Rm}^{H,H}(\omega) / \Gamma_{Rm}^{H,V}(\omega) = \Gamma_{Rm}^{V,H}(\omega) / \Gamma_{Rm}^{V,V}(\omega) = -\chi_m(\omega)$ (Haskell 1953; Harkrider 1964). Symbol $H_n^{(2)}$ in the previous expressions represents the Hankel function of second kind and order *n*, and (d , γ) are the cylindrical coordinates of any station with regard to the

source, taking the direction of L_H as the origin of the azimuthal coordinate γ (see Fig. 10).